Evolution of Structure and Interaction in Surfactant-dependent Heat-Induced Gelation of Protein

Sugam Kumar, [a,b,*] and Vinod K. Aswal[a,b,*]

[a]*Solid State Physics Division, Bhabha Atomic Research Centre, Mumbai 400 085, India*

[b]*Homi Bhabha National Institute, Mumbai 400 094, India*

**sugam@barc.gov.in; *vkaswal@barc.gov.in*

Section S1: Experimental Details. The SANS facility[S1] at the Dhruva Reactor, Bhabha Atomic Research Centre, Mumbai, India utilizes a velocity selector to provide monochromatic neutron beam (mean wavelength $\lambda \sim 5.2$ Å and width $\Delta\lambda/\lambda \sim 15\%$) which is made incident on the sample. The scatted neutrons are collected by a set of 1-d ^{3}He detectors arranged in a criss-cross geometry. The measurements were carried out in scattering vector range of 0.1 to 2.6 nm^{-1}. The collected data were corrected for background and transmission and normalized to absolute scale following the standard procedure.

The stock solutions of protein and surfactants were prepared in acetate buffer of pH 5 and then diluted to obtain required concentrations. The D_2O is used as solvent for SANS whereas samples were prepared in H_2O for other measurements. The use of the D_2O as the solvent in SANS reduces the contribution from the incoherent background and enhances the contrast for the hydrogenous scatterers like proteins/surfactants. The rheology measurements on gel samples were carried out using Anton Paar Physica MCR101 rheometer equipped with parallel plate geometry. The protein-surfactant dispersions were heated to respective critical temperatures to obtain the gels. These gels were then subjected to rheology measurements at room temperature.

Section S2: Data Analysis.

S2.1. Dynamic light scattering (DLS). DLS measurements provide plots of auto-correlation function (ACF) as a function of delay time (τ). These plots are constructed by measuring the fluctuations in the scattered light intensity, which in turn are related to the translational diffusion coefficient (D) of the particles, suspended in a medium. The normalized intensity autocorrelation function [$g^2(\tau)$] is given by following relation:[S2,S3]

$$g^2(\tau) = 1 + \beta\left|e^{-DQ^2\tau}\right|^2 \quad (1)$$

where β is the spatial coherence factor, which depends on the instrument optics and Q is the magnitude of scattering vector. [S2,S3]

For poly-dispersed system, with a narrow size distribution of scatterers, the cumulant analysis is usually used to obtain the mean diffusion coefficient.[36,37] This diffusion coefficient is then used to calculate the effective mean hydrodynamic size (D_h) of the particles/scatterers, utilizing following Stokes-Einstein's relation (k_B : Boltzmann's constant; T : absolute temperature; η : viscosity of the solvent): [S2,S3]

$$D_h = \frac{k_B T}{3\pi\eta D} \tag{2}$$

S2.2. Small-angle Neutron Scattering (SANS). In SANS, a beam of monochromatic neutrons is directed onto the sample and the intensity of scattered neutrons is measured at different scattering angles. The intensity of the scattered neutrons is related to the macroscopic differential scattering cross section (dΣ/dQ), which for a system consisting of monodispersed particles dispersed in a medium can be given by following relation:[S4,S5]

$$\frac{d\Sigma}{d\Omega}(Q) = \frac{N_p(\rho_p - \rho_m)^2 V_p^{\,2}}{V_S} P(Q)\, S(Q) \tag{3}$$

where, Q (= 4π Sinθ/λ, where 2θ is scattering angle and λ is wavelength of incident beam) is magnitude of scattering vector; N_p is the number of scatterers in the sample; V_s represents the sample volume; V_p is the volume of a single scatterers; $(\rho_p - \rho_m)^2$ is called the contrast factor and is scattering length density difference between particle (ρ_p) and matrix (ρ_m); $P(Q)$ is the intraparticle structure factor; S(Q) denotes the interparticle structure factor.

$P(Q)$ depends on the geometry (shape and size) of the scatterers (in this case, protein, micelles and their complexes). For a spherical particle of radius R and volume V, $P_s(Q)$ is given by:[S5]

$$P_S(Q) = \left[\frac{3\{sin(QR) - QR\, cos(QR)\}}{(QR)^3}\right]^2 \tag{4}$$

The expression for $P(Q)$ of ellipsoidal particle is given by

$$P(Q) = \int_0^1 F\left(Q, \mu\right)^2 d\mu \tag{5}$$

where $F(Q,\, x) = \dfrac{3(sin\, x - x\cos x)}{x^3}$ in this $x = Q\left[a^2\mu^2 + b^2\left(1-\mu^2\right)\right]^{\frac{1}{2}}$

where *a* and *b* denote the semi-axes for ellipsoid shape, μ is the cosine of the angle between the direction of major axis and scattering vector *Q*. The BSA protein is described by an oblate ($b=c>a$) ellipsoidal shape, whereas surfactant (SDS/DTAB) micelles are usually modeled by prolate ellipsoidal shape ($b=c<a$).[S5]

The interparticle structure factor $S(Q)$ contributes to the scattering intensity pattern above a particular concentration where the particles start interacting with each other. For sufficiently dilute systems, $S(Q)$ can be approximated to unity. For the systems $S(Q) \neq 1$, it is governed by correlation between the particles, which in turn depends on the interaction between the particles and hence determines the properties of the concentrated system. In general, the overall interaction in any system is governed by a combination of attractive and repulsive interactions.[S6,S7] Therefore, $S(Q)$ can be modelled using following two-Yukawa (2Y) potential comprising two terms, one accounting for repulsion (first term) and one for attraction (second term): [S6,S7]

$$\begin{aligned} \frac{V(r)}{kT} &= \infty \qquad (0 < r < \sigma) \\ &= K_1 \frac{exp[-Z_1(r/\sigma - 1)]}{r/\sigma} - K_2 \frac{exp[-Z_2(r/\sigma - 1)]}{r/\sigma} \quad (\sigma < r) \end{aligned} \tag{6}$$

where *K* (in units of $k_B T$) parameters are proportional to the strength while Z parameters are related to inverse of the range of respective parts of the interaction potential. Interparticle distance is represented by *r* while σ is hard sphere diameter of the particle. $S(Q)$ for 2Y potential is calculated numerically to obtain the strength and the range of the individual parts (attractive and repulsive) of the total potential.

The surfactant interaction with protein usually leads to the protein denaturation resulting in to the formation of beads-on-string kind of structure, where the micelle-like clusters randomly distributed along the unfolded polypeptide chain of the protein. The interparticle structure factor for such structures are usually calculated by random flight model. The $S(Q)$ for this model can be expressed as[S8, S9]

$$S(q) = \left[\frac{2}{1 - sin(qh)/(qh)} - 1 - \frac{2\left[1 - \left(sin(qh)/(qh)\right)^{N_{CLU}}\right]}{N_{CLU}\left(1 - sin(qh)/(qh)\right)^2} \frac{sin(qh)}{qh} \right] \tag{7}$$

where N_{CLU} denotes the random flight steps or in this case the number of micelles per cluster and *h* represents the step size or the distance between the centers of two micelles.

The data analysis has been carried out by fitting the experimental data with the scattering calculated for different suitable theoretical models, and the parameters were optimized by employing nonlinear least square fitting methods. Throughout the data analysis, corrections were also made for instrumental smearing.[S5]

S2.3. Circular dichroism spectroscopy. The measured ellipticity (mdeg) can be converted to Mean Residual Ellipticity (MRE) utilizing following equitation**:**[S10-S12]

$$\text{Mean Residual Ellipticity} = \frac{\text{CD(mdeg)M}}{mlC} \qquad (8)$$

Where CD is measured ellipticity in mdeg; M is molecular weight of protein in g/dmol; n is number of amino acid residues (583, in case of BSA); l is path length and C is concentration of protein in g/L.

Then content of α-helix has been obtained by employing following relation:[S10-S12]

$$\alpha - \text{helix}\ (\%) = \frac{|\text{MRE}|_{222} - 2340}{30300} \times 100 \qquad (9)$$

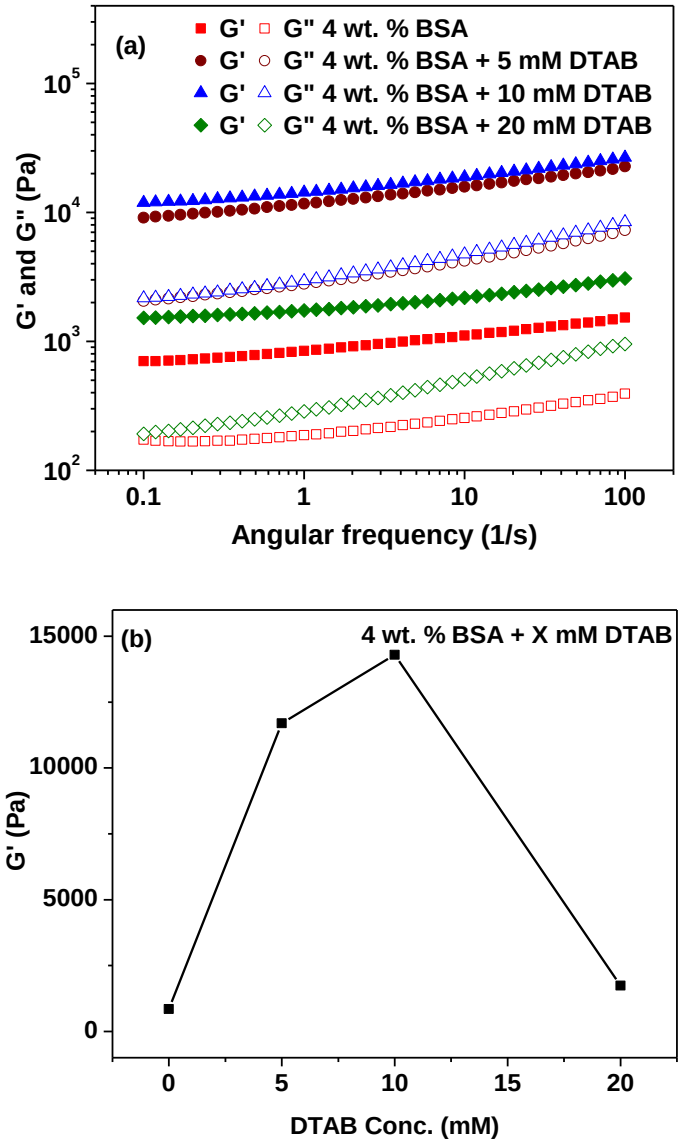

Figure S1. (a) Storage (G) and loss (G″) moduli of gel of 4 wt. % BSA + X mM DTAB (C ≤ 20 mM) samples, prepared on heating at respective critical temperature (Figure S1 of SI). (b) variation in G′ of 4 wt. % BSA + X mM DTAB (C ≤ 20 mM) samples at angular frequency (ω) of 1 s^{-1}.

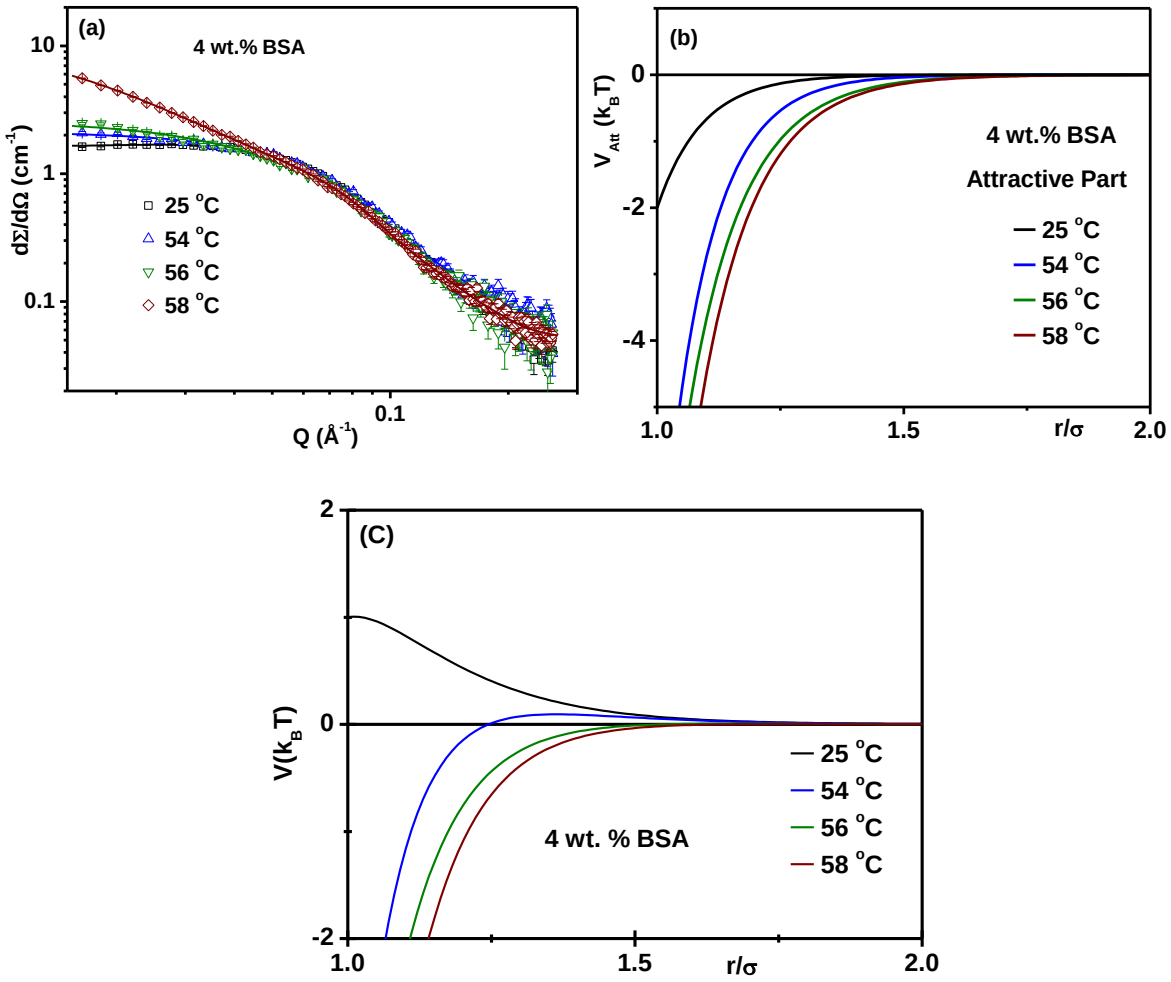

Figure S2. (a) SANS data of 4 wt. % BSA dispersion as a function of temperature. (b) Fitted attractive parts of the total potential and (c) fitted total potentials between protein molecules in 4 wt. % BSA system with increasing temperature.

Table ST1. Fitted parameters for the 4 wt. % BSA solutions with increasing temperature. The data are analyzed considering unfolded protein undergoing attractive interaction. A form factor of oblate ellipsoidal shape was utilized, and the structure factor was calculated based on a 2Y potential. At 25 °C, the parameters governing attraction were held constant to represent van der Waals forces, while those related to repulsion were subject to fitting. As the temperature increases, the parameters for repulsion were fixed at the values obtained at 25 °C, and those for attraction were allowed to float to account for additional hydrophobic attraction.

Temperature (°C)	**Semi-major axis *b*=*c* (nm)**	**Semi-minor axis *a* (nm)**	***K*$_1$ (k_BT)**	***Z*$_1$**	***K*$_2$ (k_BT)**	***Z*$_2$**
25	4.2	1.4	3.0	6.0	2.0	10.0
54	4.2	1.4	3.0	6.0	8.0	10.0
56	4.4	1.4	3.0	6.0	9.0	8.0
58	4.9	1.5	3.0	6.0	11.0	8.0

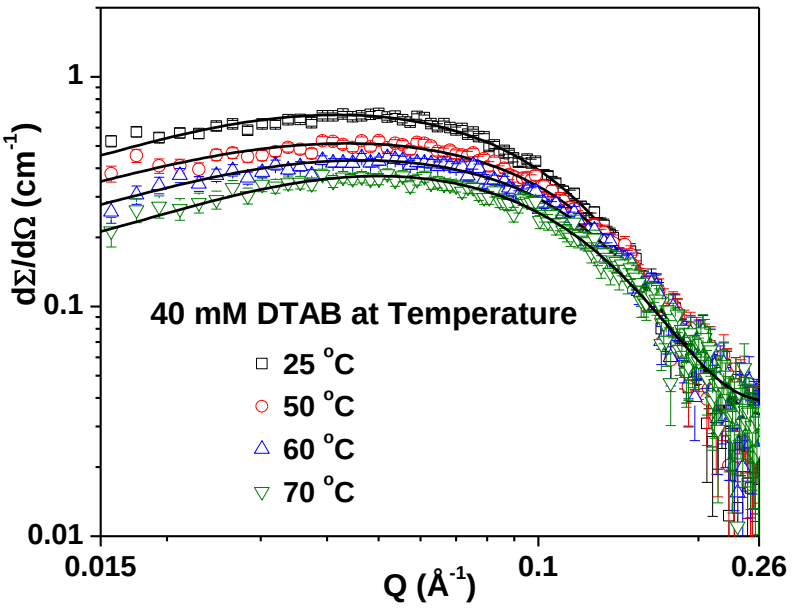

Figure S3. SANS data of 40 mM DTAB system with increasing temperature.

Table ST2. Fitted parameters for SANS data of 40 mM DTAB system with increasing temperature. Date have been modelled using P(Q) of prolate ellipsoidal micelles and S(Q) as calculated by Hayter and Penfold analysis under the rescaled mean spherical approximation for charged macroions.[13,14]

Temperature (°C)	Semi-major axis a (nm)	Semi-minor axis b=c (nm)	Charge (e.u.)	Aggregation number
25	2.8	1.6	2.2	86
50	2.5	1.6	2.5	77
60	2.3	1.6	3.0	71
70	2.0	1.6	3.5	62

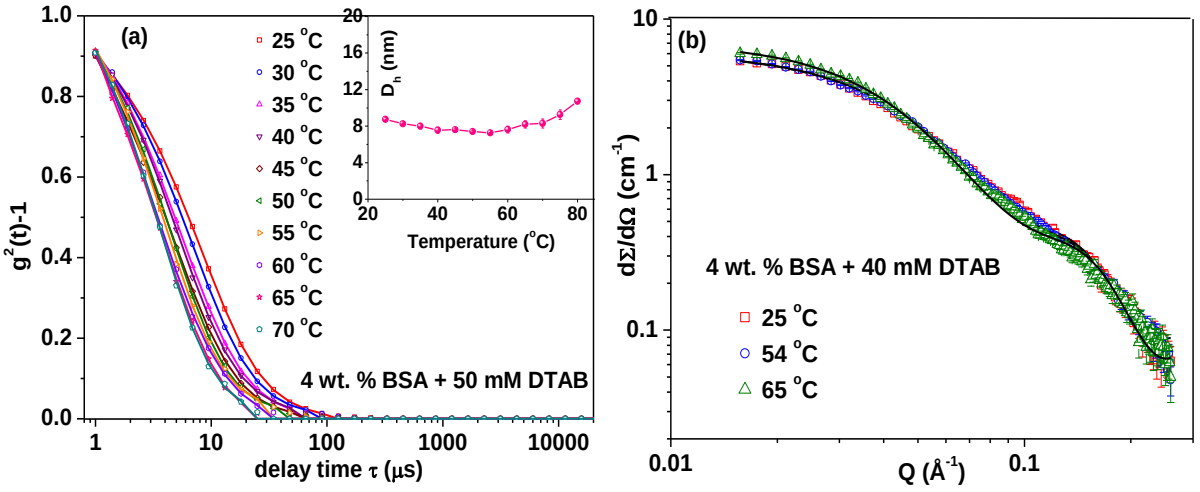

Figure S4. (a) Auto-correlation functions of 4 wt. % BSA dispersion in presence of 50 mM DTAB with increasing temperature. Inset of (a) shows variation in hydrodynamic size of same sample. (b) SANS data of 4 wt. % BSA with 40 mM DTAB sample as a function of temperature.

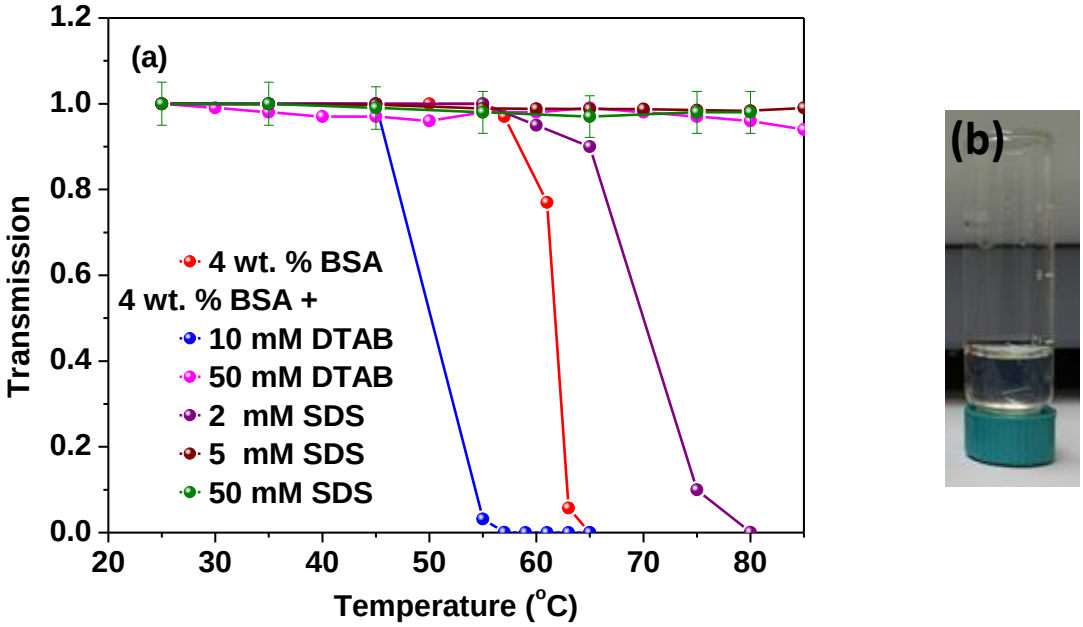

Figure S5. Measured transmission of 4 wt. % BSA in presence of different concentrations of DTAB and SDS system with increasing temperature. The decrease in transmission suggests formation of larger protein aggregates leading to protein gelation (Tr ~ 0). There is almost no decrease in the transmission of the protein-surfactant sample for DTAB and SDS concentrations more than a critical concentration, which is much less for SDS. The data suggest that presence of even 5 mM SDS can prevent the protein gelation. (b) physical state of the 4 wt. % BSA dispersion in presence of 5 mM SDS at 80 ^{o}C showing prevention of gelation.

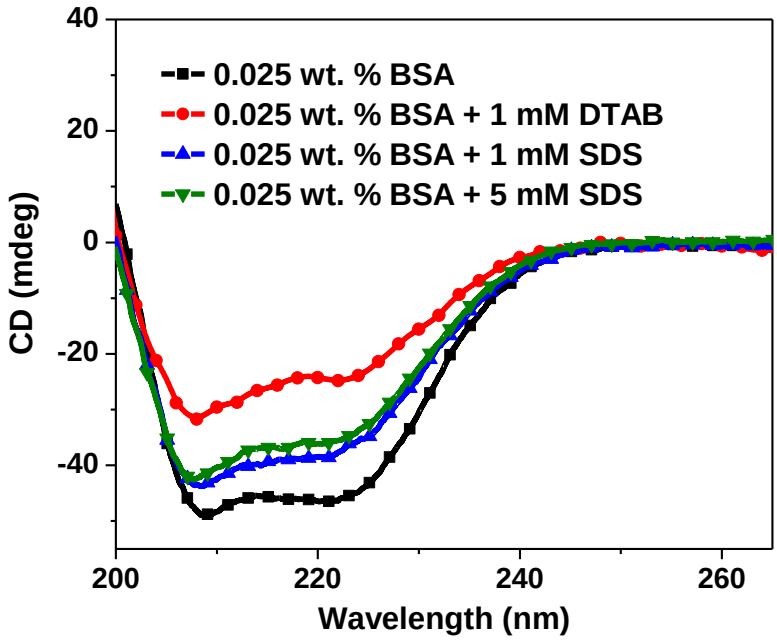

Figure S6. Circular dichroism (CD) spectra of BSA, BSA+SDS and BSA+DTAB systems.

Table ST3. Calculated α-helix content of BSA in the presence and absence of surfactants from CD data (Figure S6).

Sample	**α-helix (%)**
Pure (0.025 wt. %) BSA	61.5%
0.025 wt. % BSA + 1 mM DTAB	30%
0.025 wt. % BSA + 1 mM SDS	49%
0.025 wt. % BSA + 5 mM SDS	46%

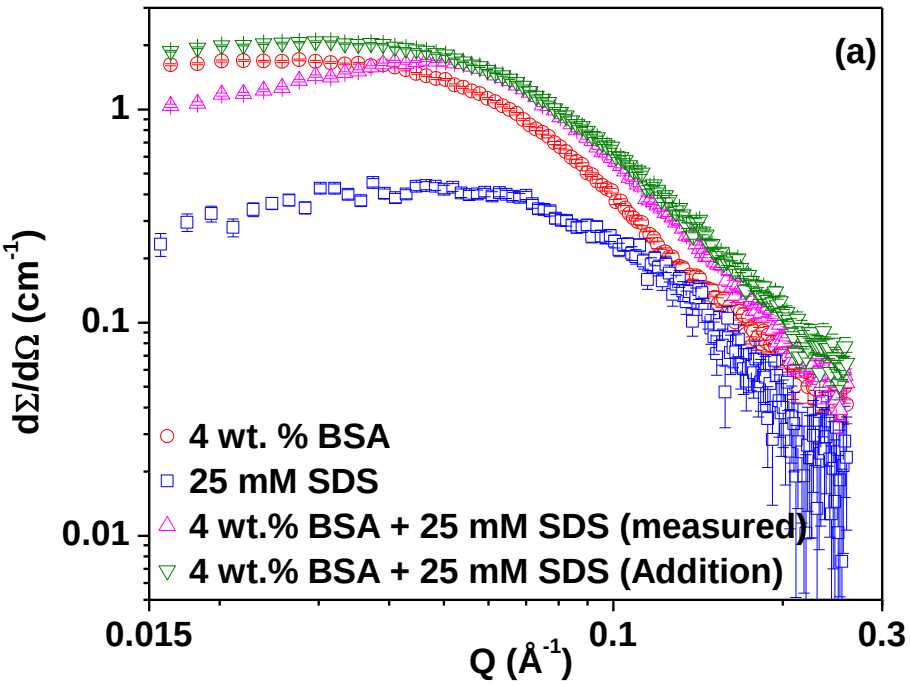

Figure S7. Comparison of the addition of individually measured (25 mM) SDS and (4 wt %) BSA data with that experimentally measured data of 4 wt% BSA + 25 mM SDS system.

Table ST4. Fitted data of 4 wt. % BSA with varying concentration of SDS at 25 °C. The shape of BSA is fitted by oblate ellipsoidal model while S(Q) is calculated for 2Y potential, where the parameters corresponding to attraction ($k_2(k_BT)$ = 2.0; Z_2= 10.0) were kept fixed, equivalent to those for pure BSA (as these are not expected to change on addition of SDS surfactant). Structural and interactional parameters of micelles were also kept fixed, equivalent to those obtained from pure SDS solutions. The parameters corresponding to the repulsion between BSA and number density of the micelles were allowed to fit.

SDS Conc. (mM)	Structural parameters of BSA		Interactional parameters of BSA		Fraction of surfactant forming free micelles (%)
	Semi-major axis *b*=*c* (nm)	Semi-minor axis *a* (nm)	K_1 (k_BT)	Z_1	
15	4.2	1.4	3.5	5.5	70
25	4.3	1.4	3.7	4.5	84
40	4.4	1.5	4.0	4.5	90

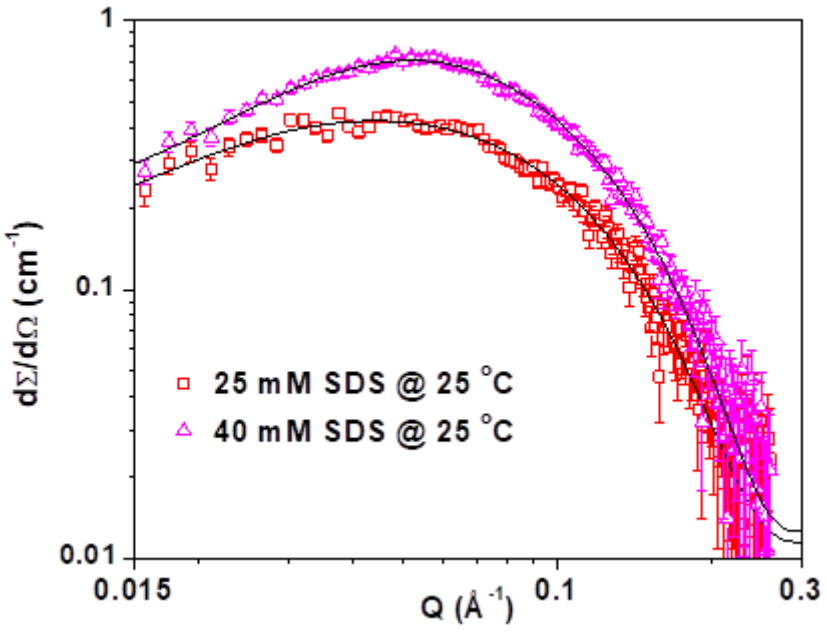

Figure S8. SANS data of the 25 mM and 40 mM SDS samples at 25 °C.

Table ST5. Fitted parameters of the pure SDS micelles. Date have been modelled using P(Q) of prolate ellipsoidal micelles and S(Q) as calculated by Hayter and Penfold analysis under the rescaled mean spherical approximation for charged macroions.[13,14]

SDS Conc. (mM)	Semi-major axis a(nm)	Semi-minor axis b=c (nm)	Charge (e.u.)	Aggregation number
25	2.7	1.5	4.2	73
40	2.9	1.6	5.4	89

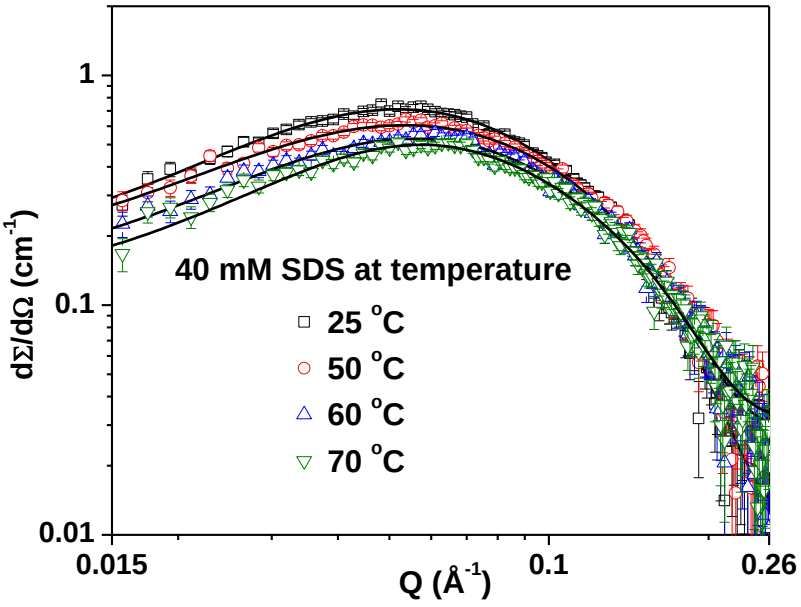

Figure S9. SANS data of 40 mM SDS system with increasing temperature.

Table ST6. Fitted parameters for SANS data of 40 mM SDS system with increasing temperature. Date have been modelled using P(Q) of prolate ellipsoidal micelles and S(Q) as calculated by Hayter and Penfold analysis under the rescaled mean spherical approximation for charged macroions.

Temperature (°C)	Semi-major axis a(nm)	Semi-minor axis b=c(nm)	Charge (e.u.)	Aggregation number
25	2.9	1.6	5.4	89
50	2.6	1.6	5.8	80
60	2.5	1.6	6.0	77
70	2.4	1.6	6.5	74

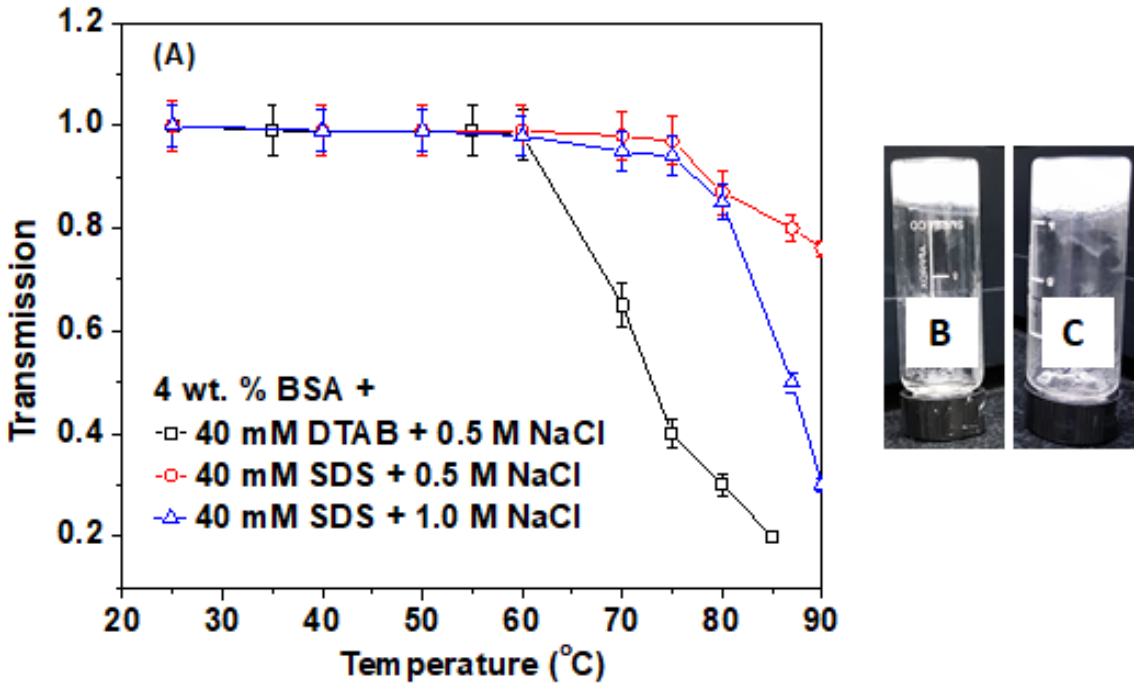

Figure S10. (A) Measured transmission of 4 wt. % BSA + 40 mM DTAB/SDS system in presence of salt with increasing temperature. It should be noted that critical/gelation temperature and salt concentration required to form gel are higher in case of BSA-SDS system compared to the BSA-DTAB. (B) and (C) show the images of the gel formed on heating of 4 wt. % BSA + 40 mM DTAB + 0.5 M NaCl and 4 wt. % BSA + 40 mM SDS + 1.0 M NaCl, samples, respectively. Sample 4 wt. % BSA + 40 mM SDS + 0.5 M NaCl does not form gel even on heating at 85 °C.

References.

S1. V. K. Aswal and P. S. Goyal, Small-angle neutron scattering diffractometer at Dhruva reactor, *Curr. Sci.* 2000, **79**, 947.

S2. S. Falke and C. Betzel, Dynamic Light Scattering (DLS). Principles, Perspectives, Applications to Biological Samples. In Radiation in Bioanalysis; Nature Publishing Group, 2019, 8, 173– 193. DOI: 10.1007/978-3-030-28247-9_6

S3. P. A. Hassan, S. Rana, G.Verma, Making sense of Brownian motion: Colloid characterization by dynamic light scattering, *Langmuir* 2015, **31**, 3.

S4. J. S. Pedersen, Analysis of small-angle scattering data from colloids and polymer solutions: Modeling and least-squares fitting, Adv. Colloid Interface Sci. 1997, 70, 171.

S5. E. Mahieu and F. Gabel, Biological small-angle neutron scattering: recent results and development. Acta Cryst. 2018, D74, 715–726

S6. Y. Liu, W.-R. Chen, S.-H. Chen, Cluster Formation in two-Yukawa Fluids. J. Chem. Phys. 2005, 122, 044507.

S7. S.-H. Chen, M. Broccio, Y. Liu, E. Fratini, and P. Baglionid, The two-Yukawa model and its applications: the cases of charged proteins and copolymer micellar solutions. J. Appl. Cryst. 2007, 40, s321–s326.

S8. W. Burchard, K. Kajiwara, The Statistics of Stiff Chain Molecules. I. The Particle Scattering Factor. *Proc. R. Soc. London, Ser. A* 1970, **316**, 185−199.

S9. D. Saha, D. Ray, J. Kohlbrecher, V. K. Aswal, Random flight model analysis of protein-surfactant complexes. AIP Conf. Proc. 2019, 2115, 030033.

S10. U. Anand and S. Mukherjee, Reversibility in protein folding: effect of b-cyclodextrin on bovine serum albumin unfolded by sodium dodecyl sulphate. Phys.Chem. Chem. Phys., 2013, 15, 9375-9383.

S11. S. Muzammil, Y. Kumar, S. Tayyab, Molten globule-like state of human serum albumin at low pH. FEBS J. 1999, 266, 26-32.

S12. Y. H. Chen, Z. T. Yang, H. Martinez, Determination of the secondary structures of proteins by circular dichroism and optical rotatory dispersion. Biochemistry 1972, 11, 4120-4131.

S13. J. B. Hayter, J. Penfold, An Analytic Structure Factor for Macroion Solutions. Mol. Phys. 1981, 42, 109−118.

S14. S. Kumar and V. K. Aswal, Tuning of nanoparticle–surfactant interactions in aqueous system. J. Phys.: Condens. Matter 23 (2011) 035101